PNAS
www.pnas.org

Supplementary Information for

Two PKA RIα holoenzyme states define ATP as an isoform-specific orthosteric inhibitor that competes with the allosteric activator, cAMP

Tsan-Wen Lu, Jian Wu, Phillip C. Aoto, Jui-Hung Weng, Lalima G. Ahuja, Nicholas Sun, Cecilia Y. Cheng, Ping Zhang, Susan S. Taylor

Susan S. Taylor
Email: staylor@ucsd.edu

This PDF file includes:

Supplementary text
Figs. S1 to S9
References for SI reference citations

Other supplementary materials for this manuscript include the following:

Movies S1 to S2
Datasets S1

MATERIAL & METHODS

Protein Purification

Human C subunit was cloned to the pET-His6-SUMO TEV LIC cloning vector (Addgene #29659). The construct was tranformmed into BL21(DE3), and induced by 0.5 mM IPTG when OD_{600}=0.6-0.8. After 16 hour expression at room temperature, the bacterial pellets were collected. The pellets were re-suspended and lysed in the lysis buffer: 20 mM Tris-Cl, 300 mM NaCl, 5 mM β-mercaptoethanol (BME). The supernatant was collected after high speed centrifugation (13,000 rpm, 1hr), and then passed through the Ni-resin. The resin was then washed with 3CV of wash buffer (20 mM Tris-Cl pH=8.0, 300 mM NaCl, 10 mM imidazole, 5 mM BME), and C-subunit was eluted by 3CV of elution buffer (20 mM Tris-Cl pH=8.0, 300 mM NaCl, 500 mM imidazole, 5 mM BME). The eluent was collected and dialyzed in dialysis buffer (20 mM Tris-Cl pH=8.0, 300 mM NaCl, 5 mM BME). After removing imidazole, the SUMO tag was cleaved by incubating with Ulp1 (molar ratio SUMO-C : Ulp1 = 200 : 1) at room temperature for 1 hour. The cleaved tag and uncleaved protein were removed by passing the solution back through the Ni-resin. The proteins were further purified by S-75 gel filtration column with buffer 20 mM MES pH=6.5, 300 mM NaCl, 5 mM BME.

R-subunit purifications are the same as literature(1, 2).

Holoenzyme Complex Formation

Holoenzyme was prepared by mixing R-subunits (1 equiv.) with excess of C-subunits (1.3 equiv.). The mixture was dialyzed against holoenzyme buffer: 50 mM MES pH=5.8, 50 mM NaCl, 5 mM $MgCl_2$, 1 mM TCEP, (and 0.5 mM ATP or ADP). Unbound C subunits was removed by S-200 gel filtration column with the same holoenzyme buffer.

Structure Determination and Refinement

Single crystals of $RI\alpha_2C_2$ Holoenzyme were grown in hanging drops using the vapor diffusion method by mixing 1 µl of the protein solution (7.5 mg/ml) and 1 µl of the reservoir solution (100 mM imidazole/MES pH=7.0, 100 mM NPS, 16.8% v/v Ethylene glycol, 8.4 % w/v PEG 8000. The original condition was from Molecular Dimension Morpheus C6 condition) at 22.5 °C. Crystals were flash frozen and the X-ray diffraction data sets were collected at the Advanced Light Source, Berkeley California beamline 8.2.2 and processed with HKL2000(3). After screening >1000 crystals, finally one crystal can diffracted to 3.55 Å resolution, which belong to a $P2_12_12_1$ space group with cell dimensions of a=139.8 Å, b=184.8 Å, and c=183.4 Å (Fig. S2B). The structure phasing was solved using the (1-91Δ)RIα:C heterodimer structure (PDB 2QCS) as a molecular replacement search model. Four RIα:C complexes (two $RI\alpha_2C_2$ holoenzymes) were found in each asymmetric unit (ASU). The structure determination and refinement were carried out using CCP4 and Phenix, respectively. Model building was performed using Coot(4). In the late stage, a twin operator of -h,l,k was used for the structure refinement using Phenix. The final model includes 2479 residues, 4 Mg ions and 2 ATP. The R and R-free are 0.256 and 0.268 respectively, and the structure model has a good geometry as evaluated with PROCHECK (Fig. S2B)(5).

Hydrodynamic Radius

The Hydrodynamic Radius of the protein constructs were determined using Gel filtration Chromatography on an Analytical Sephadex S-200 column from Amersham Pharmacia(6). Buffer conditions used included 2mM $MgCl_2$, 10mM MOPS pH 7.0, 50mM NaCl and 1mM TCEP. For the size exclusion runs with ATP, 0.2mM was also included in the above mentioned buffer composition. All runs were carried out at constant flow rate of 1.0ml/min. The experiment relied on the combination of Stokes-Einstein equation with retention theory to calculate the R_h (assuming it as a sphere)(7). A standard curve for the column was created using the Molecular Weight Kit

from Sigma Aldrich (MWGF200). The R_h of the proteins were deconstructed from the said standard curve and the Perrin Shape factor was calculated using the theoretically calculated R_g (= 0.66M1/3; where M is the Molecular Weight in Daltons)(8).

SAXS Analysis

SAXS data were collected at beamline SIBYLS at Advanced Light Source equipped with Agilent 1260 series HPLC with a Shodex analytical column. Data were collected at 298K, and sample to detector distance was set at 1.5 m at λ=1.03Å. Sample concentration was ~5 mg/mL, with 60 μL in each loading. Buffer signals were subtracted base on the measurement of averaged background scattering in each sample. The scattering files were transformed into real space pair distance distribution function *p*(r), and R_g and D_{max} were also calculated based on the *p*(r) function (9). Radius of gyration (R_g) were calculated from consecutive data throughout the FPLC and checked for consistency. All data were then scaled and merged as the final plot. Both samples have no sign of aggregation according to the Guinier analysis at low scattering angles(q). The Data were analyzed by ATSAS 2.8 (10). Two peaks were observed in Kratky plot and both data sets converge to the q axis, suggesting they are compact multiple-domains protein complexes.

Fluorophore Labeling

To label with fluorophore, the Lys7 on Human C subunit was mutated to Cys.. The mutagenesis was done using NEB Q5-site directed mutagenesis kit, and the primers were designed based on the online tool NEBBaseChanger. Purification of C-subunit Lys7Cys mutant was the same as wild-type C-subunit. The purified protein was collected and incubated with 5 equiv. of Fluorescein-5-Maleimide in labeling buffer 20mM MES pH=6.5, 300mM NaCl, 5mM BME, 4mM ATP, and 8mM $MgCl_2$. After incubation at room temperature for one hour, the labeled-protein was injected to the S-200 column to remove the excess amount of un-reacted fluorophore.

Polarization Assay

The cAMP activation assay and R-C binding of RIα and RIIβ were investigated by a fluorescence polarization assay. For R-C binding, holoenzymes were formed *in situ* by mixing 10nM of Fluorescein labeled C-subunit and 2-fold serial dilution of R-subunits from 2000nM to 0nM in buffer 20 mM MOPS pH=6.5, 75 mM KCl, 0.005% Triton X-100, 1 mM DTT, 10 mM $MgCl_2$, and 1 mM ATP/ADP as indicated. For cAMP activation assay, holoenzymes were formed *in situ* by mixing 10nM of Fluorescein labeled C-subunit with 500nM of R-subunits in buffer 20 mM MOPS pH=6.5, 75 mM KCl, 0.005% Triton X-100, 1 mM DTT, 10 mM $MgCl_2$, and 1 mM ATP/ADP as indicated. A two-fold serial dilutions of cAMP from 1,0000 to 0 nM were added into each reaction to check the holoenzyme dissociation. All reactions were incubated for at least 20 min to reach equilibrium before being measured.

Excitation and emission wavelength (485 nm and at 535 nm respectively) were used to measure its polarization. The experiments were carried out with a GENios Pro micro-plate reader (Tecan) and black flat-bottom 96-well plates. Each data was repeated at least four times and the data sets were analyzed with Prism 7. Although Due to the detection limit of the assays, the measurement of half maximal effective concentration (EC50) is not equal to the dissociation constant (K_d), however is sufficient to observe ATP and ADP difference.

System Preparation for MD

Holoenzyme complexes were prepared from either Structure A or Structure B in the asymmetric unit of $RI\alpha_2C_2$ bound with/without ATP, and two Mg^{2+} ions (Structure A/Structure B). The models were processed in Maestro (Schrodinger) where missing sidechains, counter ions, and ioniziable side chains were modeled in the Protein Preparation Wizard. Hydrogens were added and the models were solvated in a cubic box of TIP4P-EW water (11) and 150 mM KCl with a 10 Å buffer in AMBERtools (12). Parameters from the Bryce AMBER Parameter Database were used for ATP (13), phosphothreonine (14), and phosphoserine (14).

MD Simulations

AMBER16 (12) was used for energy minimization, heating, and equilibration, using the CPU code for minimization and heating and GPU code for equilibration. 500 steps of hydrogen-only minimization was followed by 500 steps of solvent minimization, 500 steps of sidechain minimization, and 5000 steps of all-atom minimization. Systems were heated from 0K to 300 K over 500 ps with 2 fs timesteps and 10.0 kcal·mol·Å position restraints on protein and ligand. Temperature was maintained by the Langevin thermostat. Constant pressure equilibration with a 10 Å non-bonded cut-off was performed with 100 ps of protein and ligand restraints followed by 100 ps without restraints. Hydrogen mass repartition was implemented to achieve a 4 fs time-step for production runs (15). Production simulations were performed on GPU enabled AMBER16 (16, 17) as above in triplicate for a total aggregate simulation time of 1.5 μs for each complex.

MD Analysis

The first 50 ns of each simulation was removed prior to analysis. Trajectories were aligned to the least dynamic regions of the protein by superposing only Cα atoms with an initial RMSF less than the mean. Helical content of each trajectory was determined by DSSP and distances calculated with built-in functions of MDtraj (18).

Cook Assay

PKA kinase activity assays were carried out by using a spectrophotometric based Cook assay with using a slightly modification.(19). RIα Holoenzyme was formed *in situ* by incubating 10 nM of C-subunit and 12 nM of RIα-subunit and incubating at 25°C for 20 minutes in the buffer: 25 mM HEPES pH=7.0, 75 mM KCl, 10 mM $MgCl_2$, 1 mM ATP, and 1 mM phosphoenolpyruvate with supplement of 15 units/ml lactate dehydrogenase, 7 u/ml pyruvate kinase, and 0.2 mM NADH. To each well of a 96-well clear bottom untreated Costar plates was added 145μl of holoenzyme solution. The two-fold serial dilutions of cAMP solution from 4096 to 4 nM were

added to each well and incubated for another 10 minutes at 25°C. The reaction was initiated by addition of 0.2 mM Kemptide (LRRASLG). The activity of free C-subunit was followed spectrophotometrically by monitoring continuous decrease in absorbance at 340 nm due to oxidation of NADH using a GeniosPro microplate reader (Tecan, Research Triangle Park, NC). Each data point was measured in quadruplicate. Data were fit with Prism 4 software (GraphPad, San Diego, CA) to determine the apparent activation constants (EC50).

IP20 Polarization Assay

The cAMP activation assay of RIα holoenzymes was measured by a fluorescence polarization assay(20). Holoenzyme was formed *in situ* by mixing with molar ratio of 1.2 mol RIα and 1 mol C subunit in buffer: 20 mM HEPES pH=7.0, 75 mM KCl, 0.005% Triton X-100, 1 mM DTT, 10 mM $MgCl_2$, and 1 mM ATP. A fluorescein-labeled 20-residue PKI(5-24) peptide (FAM-IP20) was then added into the reaction. The working concentration of C subunit was 12 nM, FAM-IP20 was 2 nM. A two-fold serial dilutions of cAMP from 2,000 to 0 nM were added to each reaction to check the holoenzyme dissociation. The polarization changes come from the FAM-IP20 binding to the C subunit. Excitation and emission wavelength (485 nm and at 535 nm, respectively) to measure its polarization. The experiments were carried out with a GENios Pro micro-plate reader (Tecan) using black flat-bottom 96-well plates. Each data was repeated at least four times and the data sets were analyzed with Prism 7.

Comparison to previous RIα and RIα:C Complexes

All previous monomeric RIα-subunit structures showed the N3A-N3A' interface independent of the D/D domain except for RIα(91-244) which is missing the CNB-B domain(21). We had previously attributed this to crystal packing, but in the free RIα dimer when nothing is competing for the CNB-B domain the N3A-N3A' interface is present and accounts for the compact conformation of the RIα dimer compared to the more extended RII dimers(2). In contrast, none of

our R:C complexes show this interface indicating that it is not dominant at least when the N-linker region is missing. However, we should emphasize that to obtain our best resolving R:C crystals previously we used an Arg333$^{RI\alpha}$Lys mutant(22).

Movie. S1. PKA RIα Holoenzyme Structure.

Movie. S2. PKA RIIβ Holoenzyme Structure.

Datasets. S1. Sequences Alignment of PKA R-subunits N3A-motif.

Fig. S1

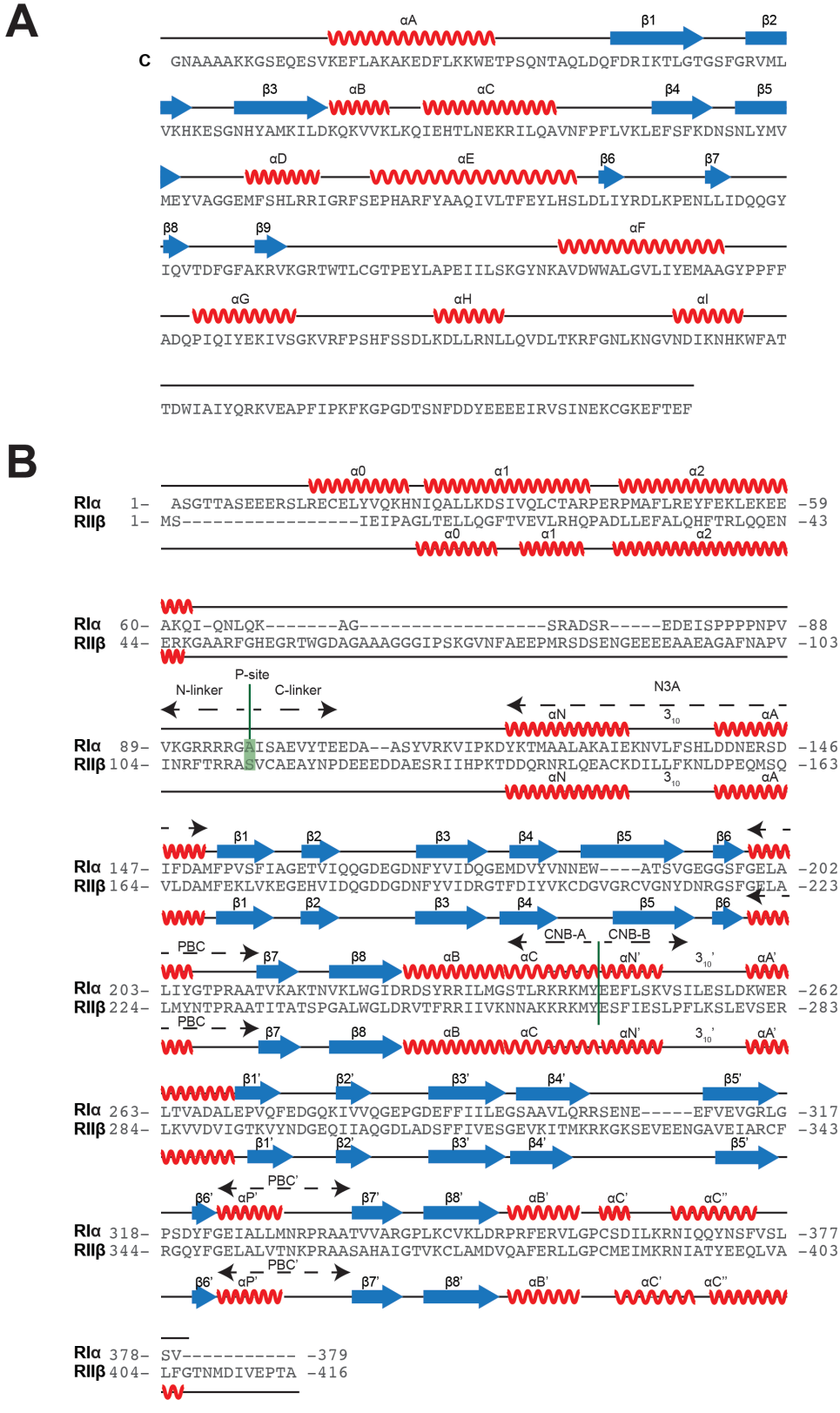

Fig. S1. PKA Sequence. (*A*) C-subunit segments nomenclatures. (*B*) RIα-, and RIIβ-subunits segments nomenclatures.

Fig. S2

A

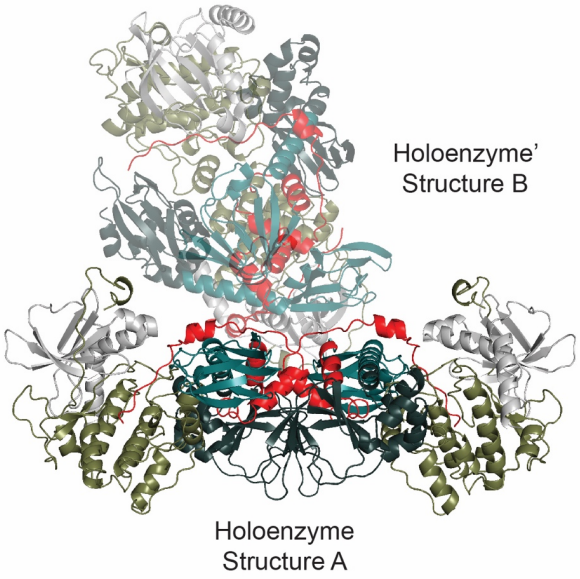

B

	$RIα_2:C_2$
Data collection	
Space group	P212121
Cell dimensions (Å)	
a	139.8
b	184.8
c	183.4
No. of molecule per Asymmetrical unit	2
Resolution (Å)	3.55
R_{merge}	0.126 (0.49)
Completeness (%)	87.0 (80.7)
I/sigma	7.6 (1.7)
No. reflections	58193
Refinement	
Resolution (Å)	50.0-3.55
R_{work} / R_{free} (%)	25.6/26.9
R.m.s. deviations	
Bond lengths (Å)	0.013
Bond angles (°)	2.0
Ramachandran angles (%)	
most favored	95.1
disallowed	None
Twin operator	-h,l,k

*Values in parentheses are for highest-resolution shell:(3.55-3.63Å)

C

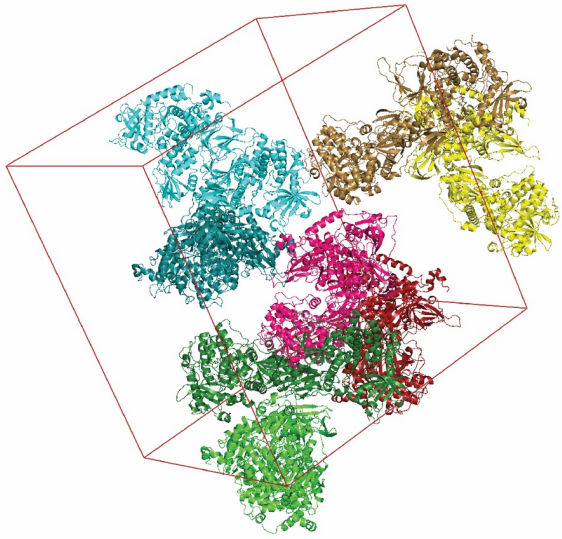

D

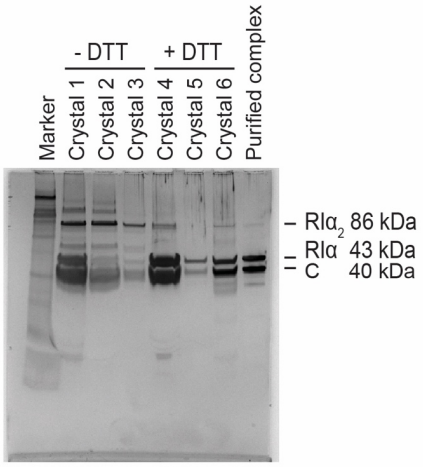

E

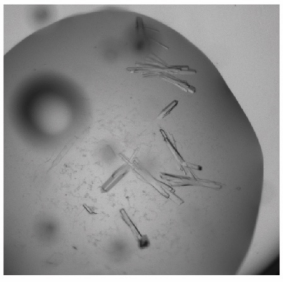

Fig. S2. Crystallography of RIα holoenzyme. (*A*) Asymmetric unit of PKA RIα holoenzyme structure. (*B*) Crystallography table. (*C*) Unit cell of PKA RIα holoenzyme structure. (*D*) Silver stained SDS-PAGE of RIα holoenzyme in crystals. (*E*) Crystals of PKA RIα holoenzyme.

Fig. S3

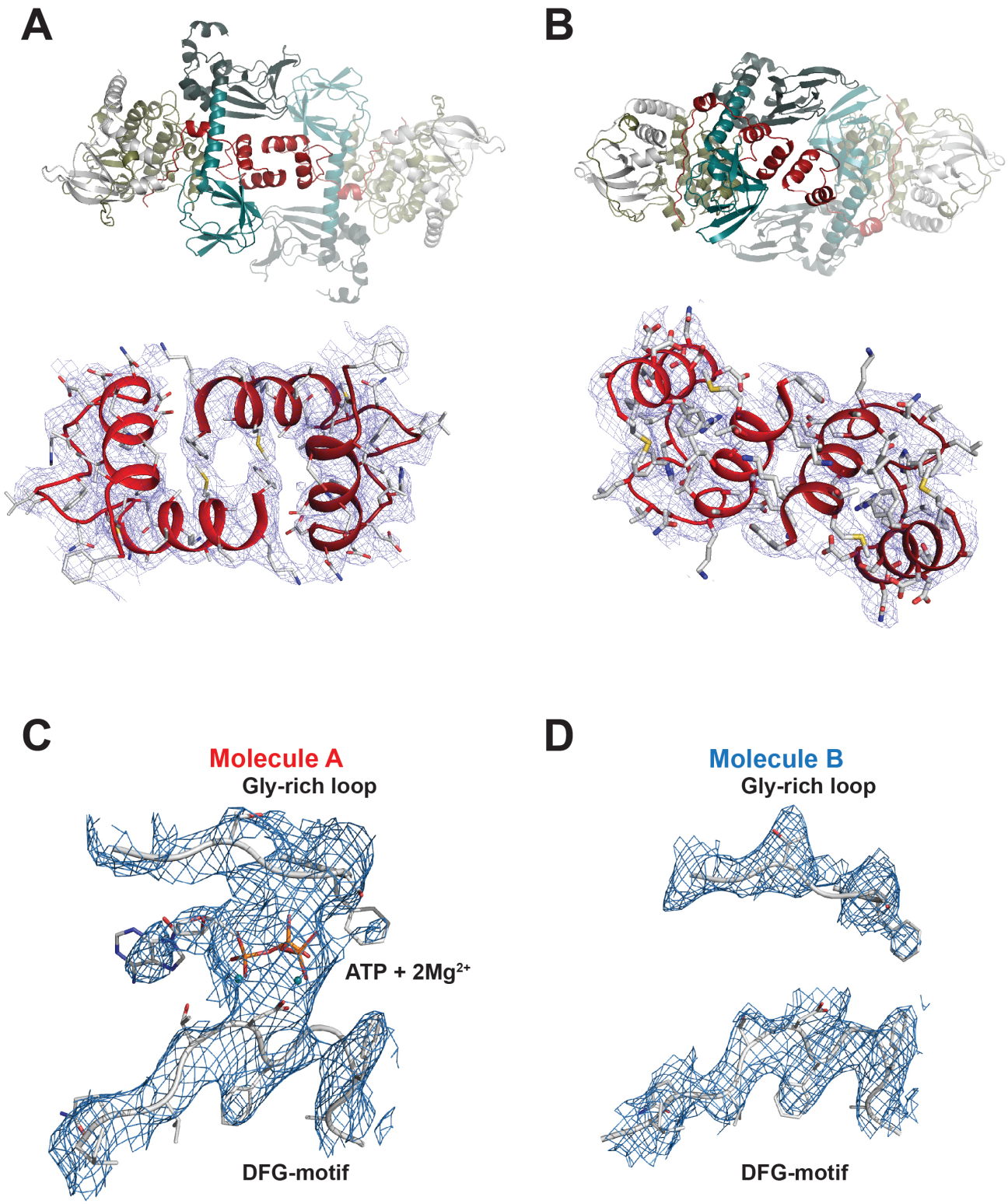

Fig. S3. Density map of RIα holoenzyme. (*A*) 2Fo-Fc density map at 1σ level of N3A-N3A' in Molecule A. (*B*) 2Fo-Fc density map at 1σ level of αN-αN' in Molecule B. (*C*) 2Fo-Fc at density map of ATP site at 0.9σ level in Molecule A. (*D*) 2Fo-Fc density map at 0.9σ level of ATP site in Molecule B.

Fig. S4

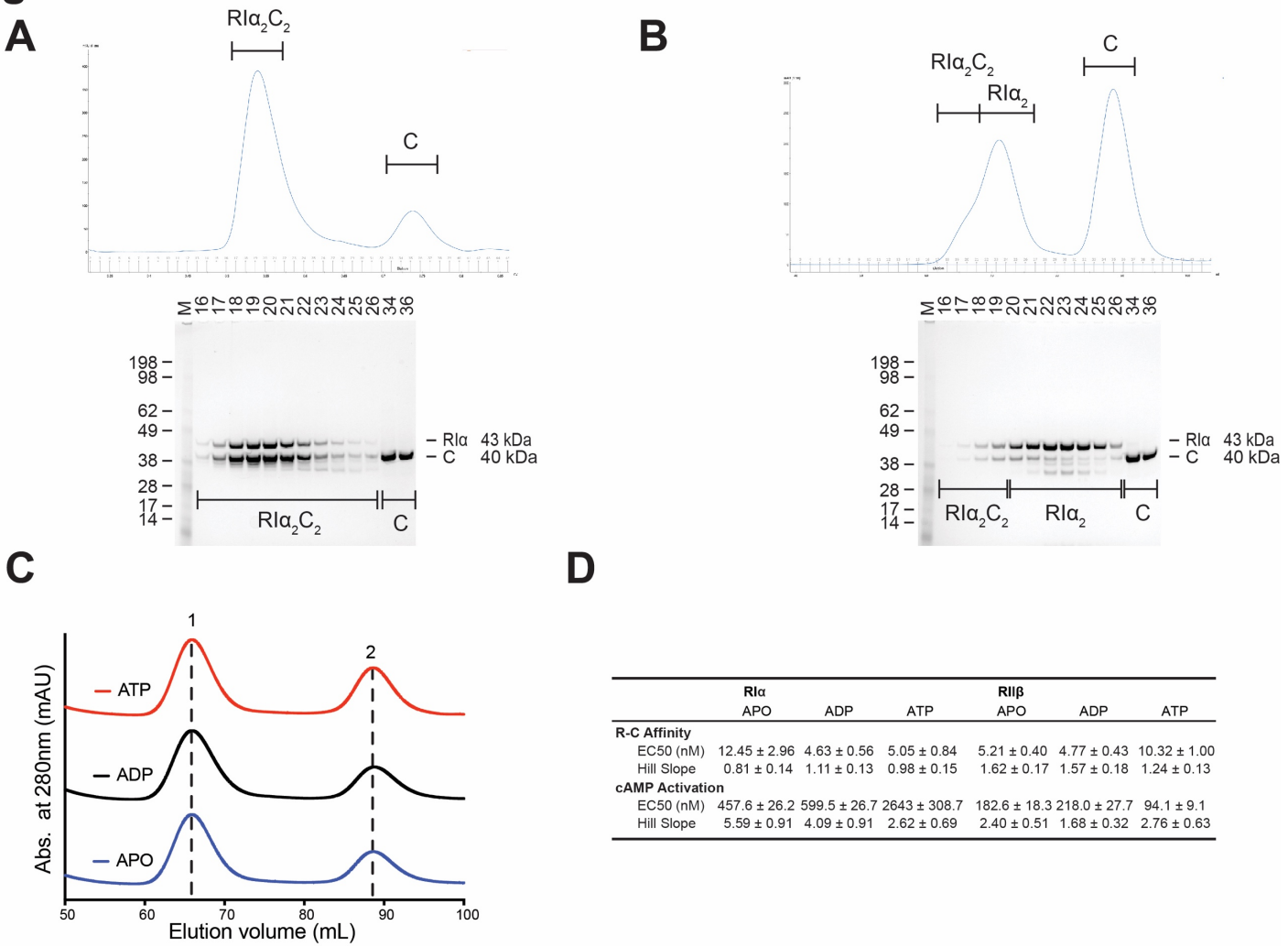

	RIα			RIIβ		
	APO	ADP	ATP	APO	ADP	ATP
R-C Affinity						
EC50 (nM)	12.45 ± 2.96	4.63 ± 0.56	5.05 ± 0.84	5.21 ± 0.40	4.77 ± 0.43	10.32 ± 1.00
Hill Slope	0.81 ± 0.14	1.11 ± 0.13	0.98 ± 0.15	1.62 ± 0.17	1.57 ± 0.18	1.24 ± 0.13
cAMP Activation						
EC50 (nM)	457.6 ± 26.2	599.5 ± 26.7	2643 ± 308.7	182.6 ± 18.3	218.0 ± 27.7	94.1 ± 9.1
Hill Slope	5.59 ± 0.91	4.09 ± 0.91	2.62 ± 0.69	2.40 ± 0.51	1.68 ± 0.32	2.76 ± 0.63

Fig. S4. RIα holoenzyme complex formation and isoform-specific properties. (*A*) Gel filtration profile and SDS-PAGE of RIα holoenzyme Molecule A formation. (*B*) Gel filtration profile and SDS-PAGE of RIα holoenzyme Molecule B formation. (*C*) Gel filtration profile of RIIβ holoenzyme in ATP (red), ADP (black), or apo (blue) condition. (*D*) The R-C affinity and cAMP activation of RIα and RIIβ.

Fig. S5

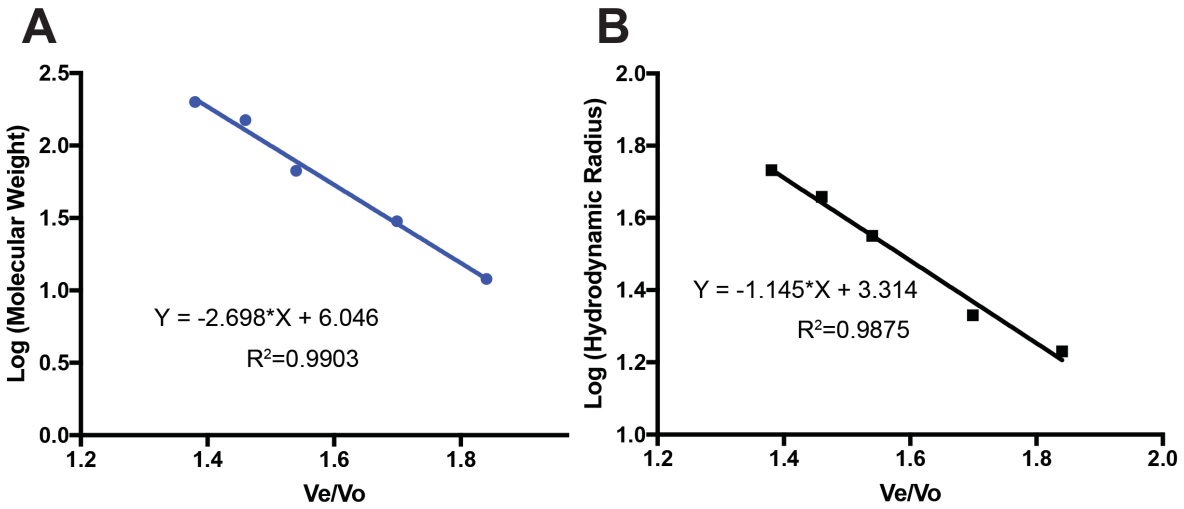

C

	Molecular Weight	Hydrodynamic Radius (Å)	Vo (mL)	Ve (mL)
Blue Dextran	2000		11.3	
Cytochrome C	12	17.0		20.8
Carbonic Anhydrase	30	21.4		19.2
Albumin	67	35.5		17.4
Alcohol Dehydrogenase	150	45.5		16.5
Beta-Amylase	200	54.0		15.6

	Ve/Vo	log (Molecular Weight)	log (Hydrodynmic Radius)
Cytochrome C	1.84	1.08	1.230
Carbonic Anhydrase	1.70	1.48	1.330
Albumin	1.54	1.83	1.550
Alcohol Dehydrogenase	1.46	2.18	1.658
Beta-Amylase	1.38	2.30	1.732

D

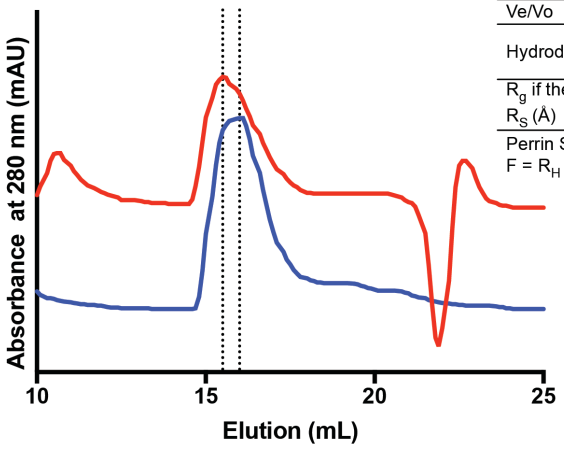

E

	Holo with ATP	Holo without ATP
Ve (mL)	15.5	16.1
Ve/Vo	1.37	1.42
Hydrodynamic Radius (Å)	55.39	48.15
R_g if the protein were a perfect sphere R_S (Å)	36.32	36.32
Perrin Shape factor $F = R_H / R_S$	1.53	1.33

Fig. S5. Hydrodynamic radius analysis of RIα holoenzyme. (*A*) The standard plot of log(molecular weight) vs. V_e/V_o. (*B*) The standard plot of log(hydrodynamics radius) vs. V_e/V_o (*C*) Elution volume and molecular weight of standards. (*D*) Gel filtration profile of RIα holoenzyme in the apo or ATP conditions. (*E*) The overview hydrodynamics and Perrin Shape factor of Molecule A and Molecule B.

Fig. S6

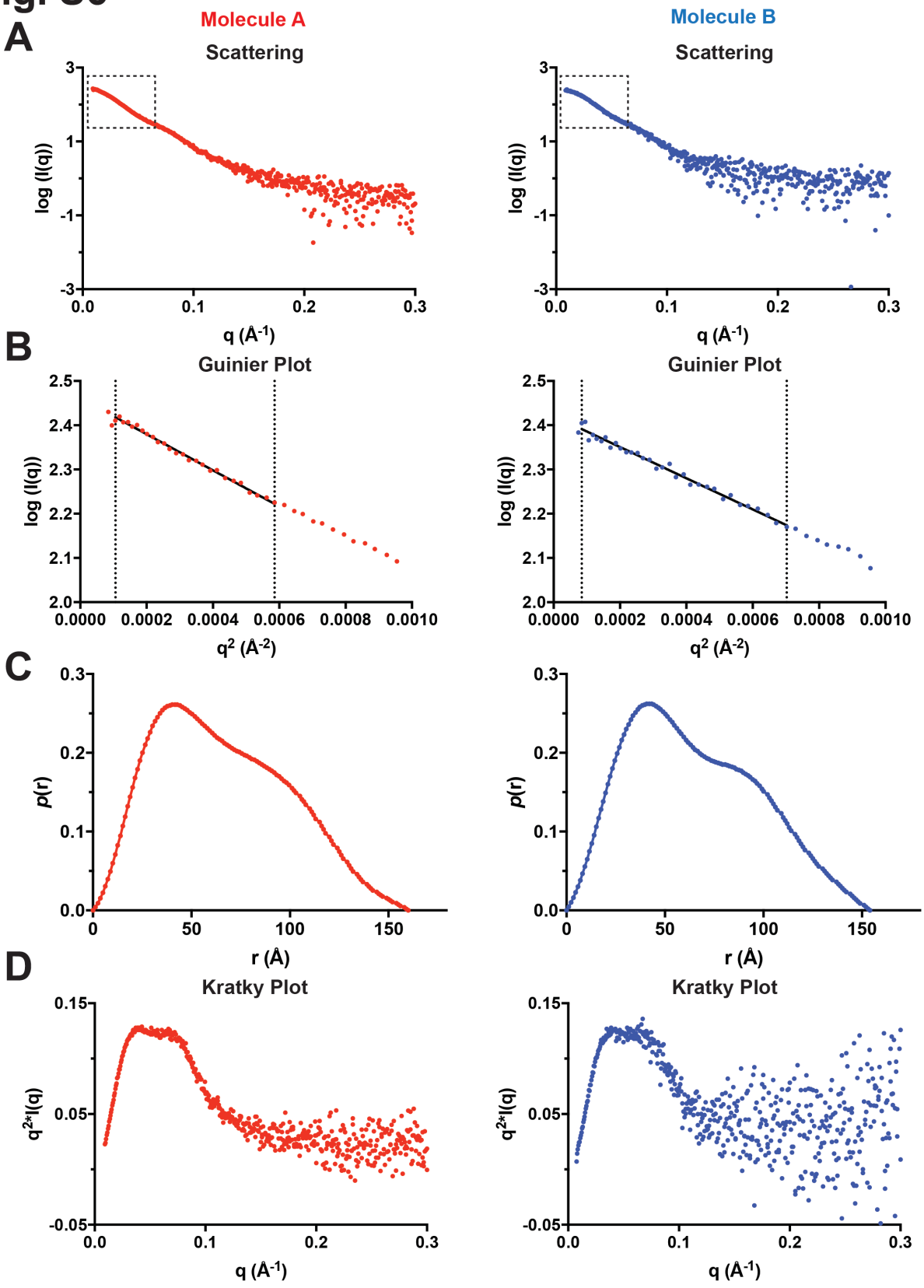

Fig. S6. SAXS analysis of RIα holoenzyme Molecule A (left, red) and Molecule B (right, blue). (*A*) Scattering profile (*B*) Guinier plot. (*C*) *P(r)* function. (*D*) Kratky plot.

Fig. S7

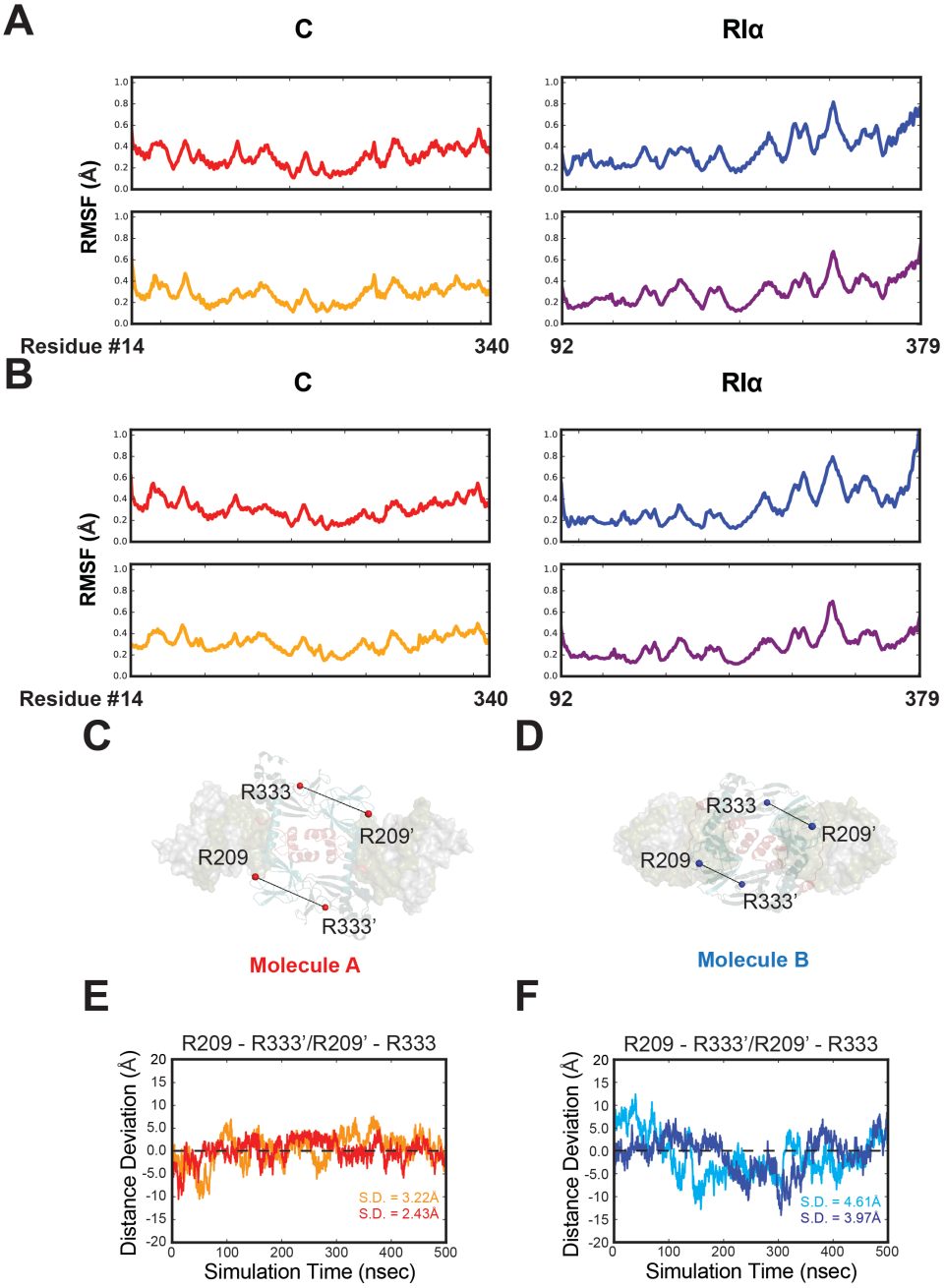

Fig. S7. MD simulations of RIα holoenzyme. (*A*) Root-Mean-Square-Fluctuation (RMSF) analysis of RIα holoenzyme Molecule A. C (red), C' (orange), RIα (blue), RIα' (purple). (*B*) Root-Mean-Square-Fluctuation (RMSF) analysis of RIα holoenzyme Molecule B. C (red), C' (orange), RIα (blue), RIα' (purple). (*C*) The representation and distance deviation of $Arg209^{RI\alpha}$-$Arg333^{RI\alpha'}$/$Arg333^{RI\alpha}$-$Arg209^{RI\alpha'}$ in Molecule A. (*D*) The distance deviation of $Arg209^{RI\alpha}$-$Arg333^{RI\alpha'}$ (red)/$Arg333^{RI\alpha}$-$Arg209^{RI\alpha'}$ (orange) in Molecule A. (*E*) The representation and distance deviation of $Arg209^{RI\alpha}$-$Arg333^{RI\alpha'}$/$Arg333^{RI\alpha}$-$Arg209^{RI\alpha'}$ in Molecule B. (*F*) The distance deviation of $Arg209^{RI\alpha}$-$Arg333^{RI\alpha'}$ (blue)/$Arg333^{RI\alpha}$-$Arg209^{RI\alpha'}$ (cyan) in Molecule B.

Fig. S8

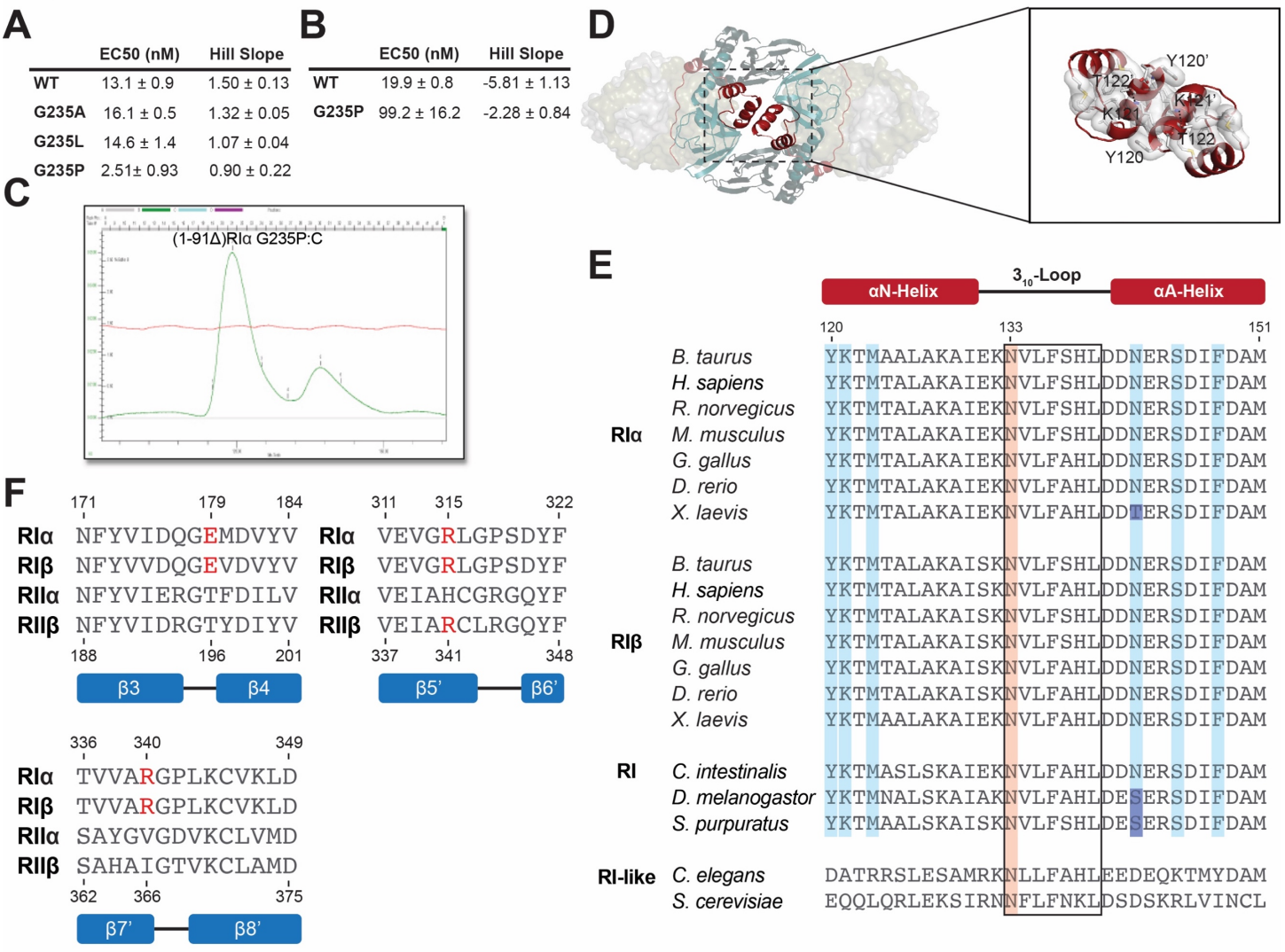

Fig. S8. αB/C/N-helix mutation and isoform-specific sequences and structures. (*A*) EC50 and Hill slope of cAMP activation in Fig. 3*H*. (*B*) EC50 and Hill slope of activity inhibition in Fig. 3*I*. (*C*) (1-91Δ)RIα(Gly235$^{RI\alpha}$Pro) form complex with C subunit. (*D*) αN-αN' interface in Molecule B. (*E*) Sequence alignments of RIα N3A motif in different species. (*F*) Sequence alignments of RIα, RIβ, RIIα, and RIIβ in CNB-A and CNB-B' interface regions.

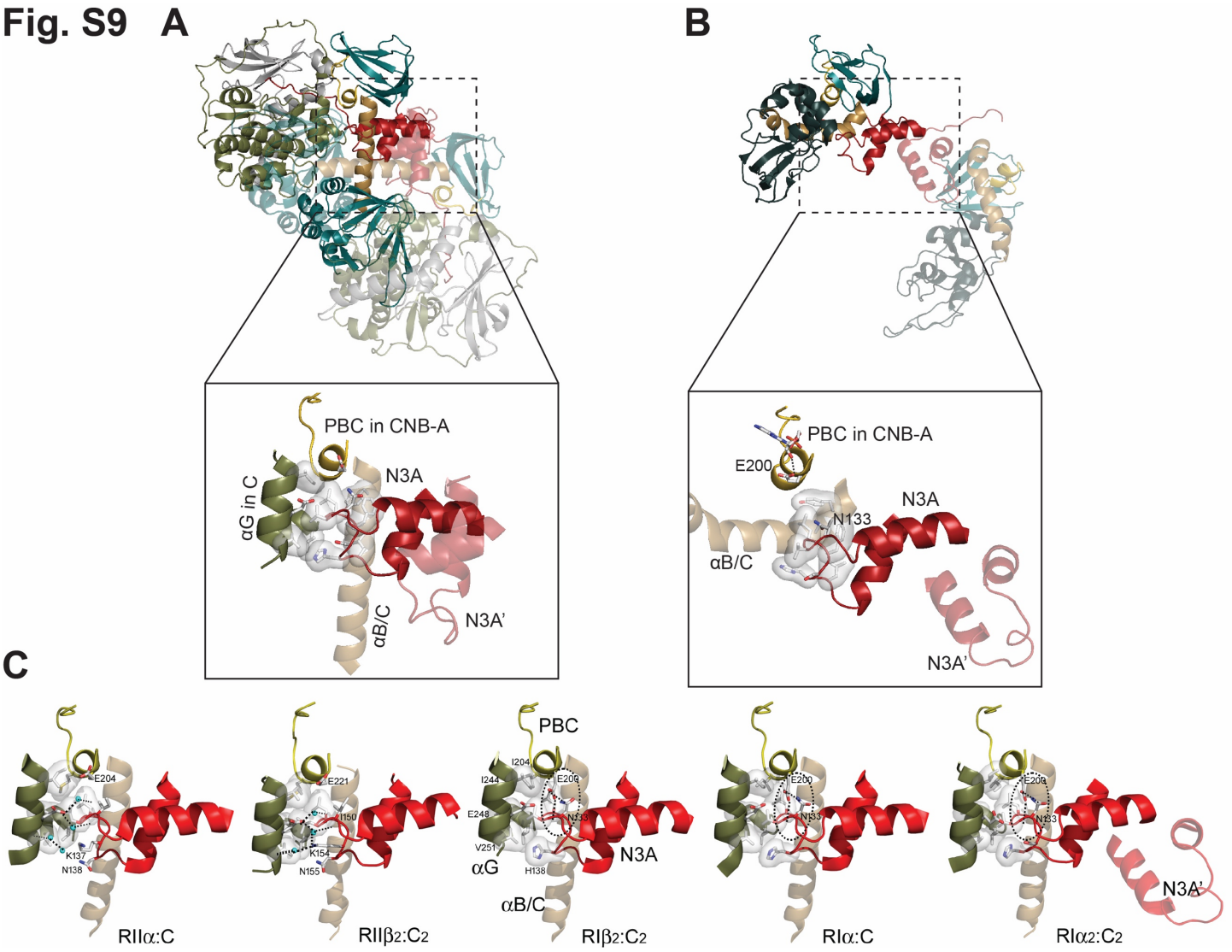

Fig. S9. Isoform-specific structures. (*A*) The 3_{10}-loop, αB/C/N-helix, and C subunit interface in Molecule B. (*B*) The 3_{10}-loop, αB/C/N-helix, and C subunit interface in RIα$_2$. (*C*) PBC, 3_{10}-loop and C subunit interface in different R isoforms structures.

Reference

1. Zhang P*, et al.* (2012) Structure and allostery of the PKA RIIbeta tetrameric holoenzyme. *Science* 335(6069):712-716.
2. Bruystens JG*, et al.* (2014) PKA RIalpha homodimer structure reveals an intermolecular interface with implications for cooperative cAMP binding and Carney complex disease. *Structure* 22(1):59-69.
3. Otwinowski Z & Minor W (1997) Processing of X-ray diffraction data collected in oscillation mode. *Methods Enzymology* 276:307-326.
4. Emsley P & Cowtan K (2004) Coot: model-building tools for molecular graphics. *Acta Crystallogr D Biol Crystallogr* 60(Pt 12 Pt 1):2126-2132.
5. Laskowski RA, MacArthur MW, Moss DS, & Thornton JM (1993) PROCHECK: a program to check the stereochemical quality of protein structures. *Journal of Applied Crystallography* 26:283-291.
6. Andrews P (1965) The gel-filtration behaviour of proteins related to their molecular weights over a wide range. *Biochem J* 96(3):595-606.
7. Wittgren B & Wahlund K-G (1997) Fast molecular mass and size characterization of polysaccharides using asymmetrical flow field-flow fractionation-multiangle light scattering. *Journal of Chromatography A* 760(2):205-218.
8. Neurath H, Cooper GR, & Erickson JO (1941) THE SHAPE OF PROTEIN MOLECULES: II. VISCOSITY AND DIFFUSION STUDIES OF NATIVE PROTEINS. *Journal of Biological Chemistry* 138(1):411-436.
9. Kikhney AG & Svergun DI (2015) A practical guide to small angle X-ray scattering (SAXS) of flexible and intrinsically disordered proteins. *FEBS Lett* 589(19 Pt A):2570-2577.

10. Franke D*, et al.* (2017) ATSAS 2.8: a comprehensive data analysis suite for small-angle scattering from macromolecular solutions. *J Appl Crystallogr* 50(Pt 4):1212-1225.

11. Horn HW*, et al.* (2004) Development of an improved four-site water model for biomolecular simulations: TIP4P-Ew. *J Chem Phys* 120(20):9665-9678.

12. D.A. Case RMB, D.S. Cerutti, T.E. Cheatham, III, T.A. Darden, R.E. Duke, T.J. Giese, H. Gohlke, A.W. Goetz, N. Homeyer, S. Izadi, P. Janowski, J. Kaus, A. Kovalenko, T.S. Lee, S. LeGrand, P. Li, C. Lin, T. Luchko, R. Luo, B. Madej, D. Mermelstein, K.M. Merz, G. Monard, H. Nguyen, H.T. Nguyen, I. Omelyan, A. Onufriev, D.R. Roe, A. Roitberg, C. Sagui, C.L. Simmerling, W.M. Botello-Smith, J. Swails, R.C. Walker, J. Wang, R.M. Wolf, X. Wu, L. Xiao and P.A. Kollman (2016) AMBER (University of California, San Francisco).

13. Meagher KL, Redman LT, & Carlson HA (2003) Development of polyphosphate parameters for use with the AMBER force field. *J Comput Chem* 24(9):1016-1025.

14. Homeyer N, Horn AHC, Lanig H, & Sticht H (2006) AMBER force-field parameters for phosphorylated amino acids in different protonation states: phosphoserine, phosphothreonine, phosphotyrosine, and phosphohistidine. *Journal of Molecular Modeling* 12(3):281-289.

15. Hopkins CW, Le Grand S, Walker RC, & Roitberg AE (2015) Long-Time-Step Molecular Dynamics through Hydrogen Mass Repartitioning. *J Chem Theory Comput* 11(4):1864-1874.

16. Le Grand S, Gotz AW, & Walker RC (2013) SPFP: Speed without compromise-A mixed precision model for GPU accelerated molecular dynamics simulations. *Computer Physics Communications* 184(2):374-380.

17. Salomon-Ferrer R, Gotz AW, Poole D, Le Grand S, & Walker RC (2013) Routine Microsecond Molecular Dynamics Simulations with AMBER on GPUs. 2. Explicit Solvent Particle Mesh Ewald. *J Chem Theory Comput* 9(9):3878-3888.

18. McGibbon RT*, et al.* (2015) MDTraj: A Modern Open Library for the Analysis of Molecular Dynamics Trajectories. *Biophysical Journal* 109(8):1528-1532.

19. Cook PF, Neville ME, Jr., Vrana KE, Hartl FT, & Roskoski R, Jr. (1982) Adenosine cyclic 3',5'-monophosphate dependent protein kinase: kinetic mechanism for the bovine skeletal muscle catalytic subunit. *Biochemistry* 21(23):5794-5799.

20. Saldanha SA, Kaler G, Cottam HB, Abagyan R, & Taylor SS (2006) A Novel Assay Principle for Modulators of Protein-Protein Interactions and its Application to non-ATP-Competitive Ligands Targeting Protein Kinase A. *Analytical Chemistry* 78(24):8265-8572.

21. Badireddy S*, et al.* (2011) Cyclic AMP analog blocks kinase activation by stabilizing inactive conformation: conformational selection highlights a new concept in allosteric inhibitor design. *Mol Cell Proteomics* 10(3):M110 004390.

22. Kim C, Cheng CY, Saldanha SA, & Taylor SS (2007) PKA-I holoenzyme structure reveals a mechanism for cAMP-dependent activation. *Cell* 130(6):1032-1043.